September 20-23, 2011
City of Cuernavaca México
XI International
Hydrogen Congress
an event of The Mexican Hydrogen Society
Cuernavaca...
The Endless Spring

Stirring method and temperature: their effect on the synthesis of metallic (M) and bimetallic (M-Pt) nanostructures

Nora Mayté Sánchez-Padilla[1], Sagrario M. Montemayor[1,*], F.J. Rodríguez Varela[2,*]

[1]Universidad Autónoma de Coahuila, V. Carranza s/n, Saltillo, Coahuila, México, CP 25280
[2]CINVESTAV-Saltillo, Carr. Saltillo-Monterrey km. 13.5, Ramos Arizpe, Coahuila, CP 25900
[*]Contact e-mails: smmontemayor@gmail.com; javier.varela@cinvestav.edu.mx

ABSTRACT

In this work, the effect of changing the stirring method and temperature on the physicochemical properties of metallic nanoparticles and bimetallic nanostructures is shown. Magnetic (MS), mechanical (UT) and ultrasonic (USS) stirring were the methods of synthesis. The effect that, temperatures between 0 and 50 °C, has on the structure and particle size of Pd, Fe and Ru nanoparticles was evaluated. The results indicate that Pd and Fe prepared by the three methods present a crystalline structure. On Fe samples, an increase of the temperature of synthesis leads to highly crystalline powders while on Pd this effect is the opposite. Meanwhile, the Ru material shows quasi-amorphous characteristics. Afterwards, Pt was deposited by the UT method on Pd (prepared by UT) and Fe (prepared by UT and USS) nanoparticles to form bimetallic Pd-Pt and Fe-Pt nanostructures. XRD characterization of the nanostructures shows crystalline patterns with peaks related to the cubic structure of Pt in all samples. The electrochemical characterization indicates a 13 or 9 times larger electrochemically active surface area of Pd-Pt related to the Fe-Pt materials, depending on method of synthesis. Furthermore, a higher catalytic activity for the ORR was measured for the Pd-Pt material compared to those of the Fe-Pt catalysts.

Key words: platinum bimetallic materials, core@shell nanostructures, oxygen reduction reaction.

1. INTRODUCTION

Worldwide, much attention has been paid to the synthesis and characterization of bimetallic nanostructures due to the possibility that catalytic properties of such materials can be tailored by changes in their composition and morphology. Some technological areas which are benefited, with a good control in the composition, structure and size of the bimetallic structures, are catalytic reforming, pollution control and electrocatalysis in fuel cells. It is well known that the composition and the structure, especially on the surface of materials, can be modified by changing reaction conditions. This, in the nanometric scale, leads to exponential changes because of the large relation surface/size. There are several ways to synthesize metallic nanoparticles and bimetallic nanostructures which involve the use of numerous and time-consuming steps of heating, handling and purification of the intermediates and products [1-3]. These drawbacks make difficult scaling up whichever of those synthesis methods.

From an application point of view, systems having bimetallic, core@shell and pseudo core@shell structures with high catalytic activity as anodes or cathodes in low temperature fuel cells have been developed recently by different synthesis routes [2, 4, 5]. Some methods demonstrate that the synthesis process can be simple, although relatively time-demanding [7].

In the course to find a simple synthesis method to obtain metallic nanoparticles and bimetallic nanostructures, which will allow to have a good control of the structure and lead to materials with interesting catalytic properties, here we studied the effect of the stirring method and the temperature on the reduction of metallic salts using $NaBH_4$. We aim to obtain core@shell (Fe_3O_4@Pt and Pd@Pt) nanostructures and to evaluate their catalytic activity towards the ORR in acid medium. Moreover, it is important to mention that the time we used for the synthesis, both of nanoparticles (cores) and bimetallic (core@shell) nanostructures was very short, i.e., only one minute.

2. EXPERIMENTAL PART

The reagents used to obtain the nanoparticles were $Fe(NO_3)_3 \cdot 9H_2O$, $PdCl_2$ and $RuCl_3$ as metallic sources and $NaBH_4$ as reducing agent. All chemicals were purchased from Aldrich. In a typical synthesis process, the stoichiometric amount of a 0.002 M metallic salt solution was added dropwise into a 0.001 M $NaBH_4$ solution at 25 °C. Each one of the salts was added into the reducing agent under three different type of stirring: magnetic (MS), mechanical (UT) and ultrasonic (USS). The nanoparticles obtained were washed and separated by centrifugation at 3000 rpm. Then, the powders were characterized by XRD to determine the structural parameters and crystallite size.

To obtain the nanostructures, the UT method was used. An appropriate amount of 0.002M $H_2PtCl_6 \cdot 6H_2O$ was added dropwise into a 0.001M $NaBH_4$ solution which contained 0.1 g of the nanoparticles prepared by UT or USS. This way, Pd-Pt, Fe-Pt and Fe-Pt bimetallic nanostructures were synthesized. The nanocatalysts were also characterized by XRD. Figure 1 shows a schematic diagram of the experimental procedure followed during the synthesis of metallic and bimetallic nanostructures.

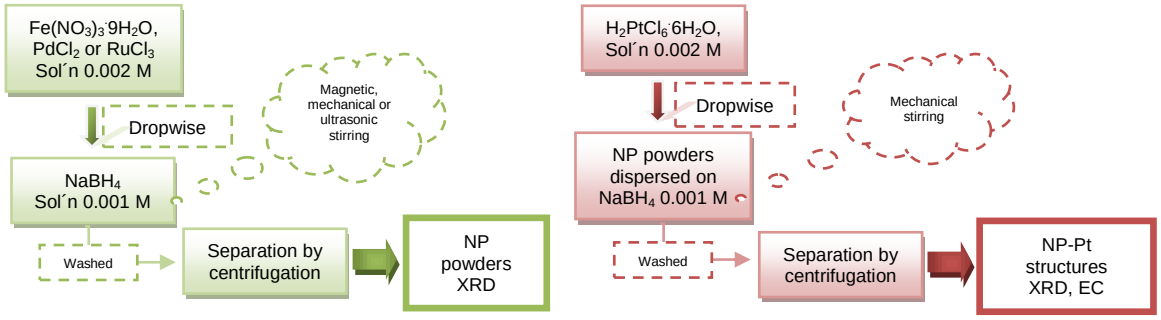

Figure 1. Flowchart of the experimental part to obtain nanoparticles (left) and nanostructures (nanoparticles-platinum) (right).

The catalytic activity of the bimetallic nanostructures for the ORR was evaluated with the aid of a potentiostat (Voltalab) connected to a RDE instrument (Pine Inst.). Cyclic voltamperograms (CV) were obtained in N_2-saturated 0.5 M H_2SO_4, while linear scan voltamperograms (LSV) were measured in O_2-saturated electrolytes at different rotating rates. The methods used to prepare catalytic inks and working electrodes has already been described with detail elsewhere [6].

3. RESULTS AND DISCUSSION

The first evidence of the effect of $NaBH_4$ on the metal precursors was the formation of a black colloidal suspension; this was observed using any of the three metallic salts and the three stirring methods proposed. The X-ray diffraction patterns of the resulting powders show that each experiment gives place to different results.

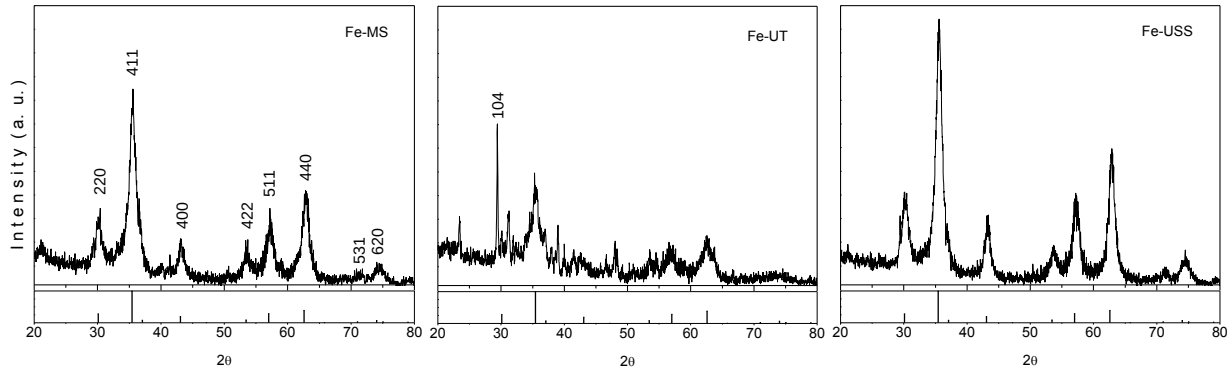

Figure 2. XRD patterns showing the effect of stirring method on the Fe_3O_4 nanoparticles.

For example, when Fe^{3+} is used, the reducing agent does not avoid the formation of iron oxide. Figure 2 shows the XRD patterns of iron oxide nanoparticles obtained using MS, UT and USS. A spinel-type cubic phase identified as magnetite ($FeO{\cdot}Fe_2O_3$, PDF 89-0691) is present in all cases, although the intensity of the reflections is lower or higher as a function of the stirring method. An additional peak in the diffractogram of the powder obtained by UT at about 2θ=29.3

is related to $NaNO_3$ formed as secondary phase which was not completely removed as the sample was washed. The crystallite sizes, calculated using the Scherrer equation, are in the range from 5 to 8 nm, the largest one corresponding to the sample obtained by the USS process.

On the contrary, when Pd^{2+} is used, $NaBH_4$ reduces completely the divalent palladium to elemental palladium, as it can be seen in the Figure 3. Irrespective of the stirring method, all reflections present in the diffractograms are related to the Pd cubic structure (PDF 46-1043 chart). It is important to mention that especial care was taken to control the temperature, although it was easier for MS than for USS. There are not significant differences between the intensity of the peaks or crystallite sizes, which are of 9 nm for three cases, in the patterns in Figure 3.

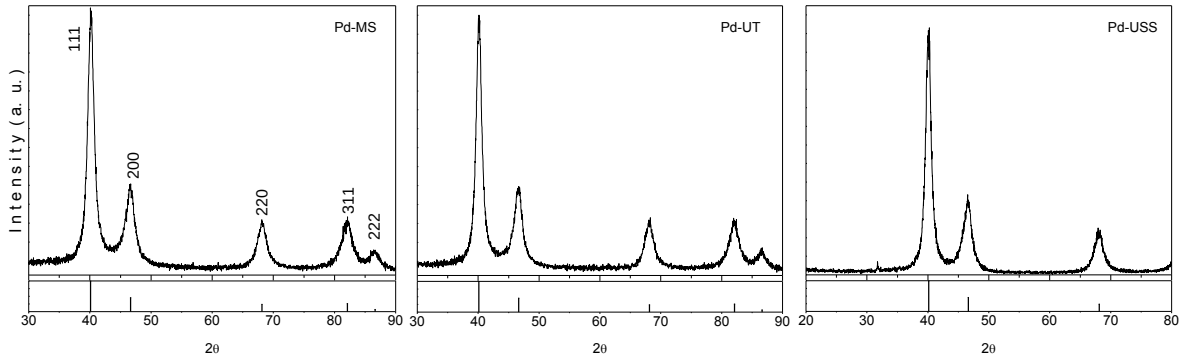

Figure 3. patterns showing the effect of stirring method on the Pd nanoparticles.

The reaction of Ru^{3+} with the reducing agent gives place to a quasi-amorphous material, at room temperature and under MS, MT and USS stirring. An example of the diffractograms obtained is shown in Figure 4. In future works, the use of different conditions of synthesis will be evaluated in order to obtain polycrystalline Ru powders. Needless to say that, the Scherrer formula, cannot be used in these cases.

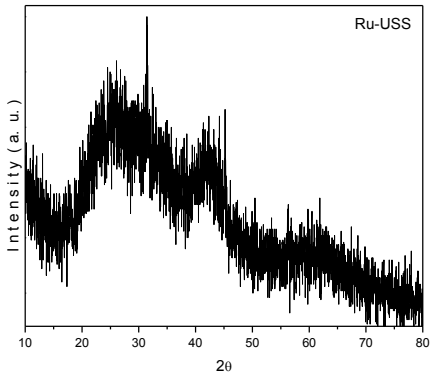

Figure 4. Quasi-amorphous powder obtained using $RuCl_3$ as precursor.

The effect of the temperature on the crystallinity of the Fe_3O_4 and Pd nanoparticles is shown in the Figure 5. Similar to the stirring method, the use of different temperatures, result in noticeable changes in the XRD patterns in each case. On the one hand, the crystallinity of the iron oxide is better when the temperature is higher during the synthesis although the crystallite size also increases. The diffractograms on the upper level in the figure show the patterns of Fe_3O_4 obtained to 0 (left) and 50 °C (right). The effect of a decrease in the temperature on the crystallite size is evident. At 0 °C the crystallites are only of 4.4 nm of diameter, while the increase of temperature from 25 to 50 °C seems not to affect considerably the crystallite size which is of 9.2 nm.

On the other hand, the patterns at the bottom level in Figure 5 show the Pd nanoparticles synthesized to 0 and 50 °C in the left and right side, respectively. An opposite effect related to Fe_3O_4 can be observed on the crystallinity of the Pd nanoparticles, i.e., when a higher temperature is used the crystallinity is poorer. In this case, however, the crystallite size of the sample at higher temperature does not change with respect to the sample obtained at room temperature. Both systems in Figure 5, Fe_3O_4 and Pd, were synthesized by UT stirring.

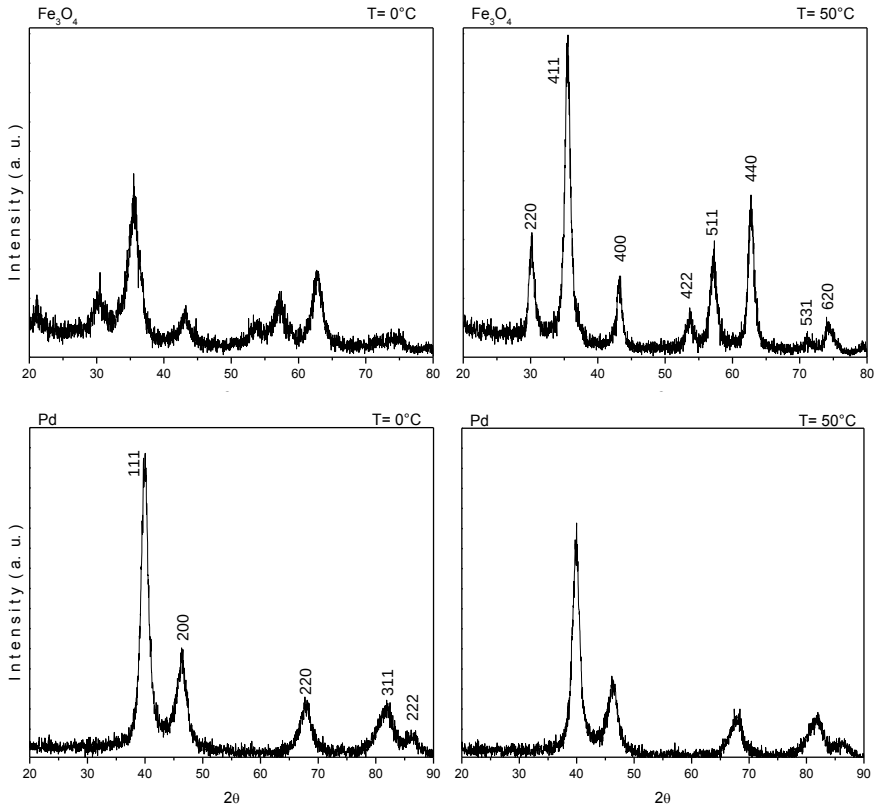

Figure 5. Effect of the temperature on the crystallinity of Fe_3O_4 (top) and Pd (bottom) nanoparticles.

The second step of this simple synthesis route takes place on the magnetite (produced by MS and USS) and palladium (produced by UT) to form a second crystalline phase. As an example, Figure 6 shows the XRD patterns of Fe_3O_4-Pt (left) and Pd-Pt (right), where Pt was deposited using UT stirring.

The main peaks related to the cubic structure of platinum, PDF 4-0802, are present in all samples. The bimetallic Fe_3O_4-Pt nanostructures have both reflections sets, i.e., those associated to the magnetite spinel structure and those assigned to the cubic close-packed structure of Pt. This is considered to be a result of the large differences between both crystal structures and their cell parameters. In contrast, for the Pd-Pt bimetallic system, only one set of reflections seems to appear. This is due to the fact that both Pd and Pt have cubic close-packed structures and similar

cell parameters differing by only 0.03 Å. A careful observation of all reflections allows to detect a shift of the signals, with respect to Pd standard, as a consequence of the presence of polycrystalline Pt.

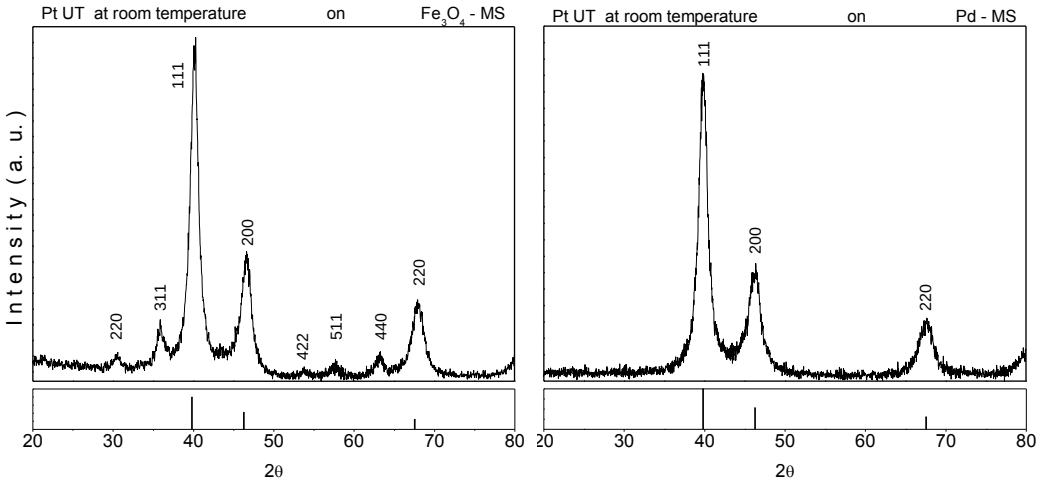

Figure 6. XRD patterns of (nanoparticles)-Pt systems. Left: Fe_3O_4-Pt, right: Pd-Pt.

Three bimetallic nanostructures were selected for electrochemical characterization: i) Fe_3O_4(UT)-Pt; ii) Fe_3O_4(USS)-Pt; and iii) Pd(UT)-Pt. All nanostructures were prepared by depositing Pt on the corresponding nanoparticle by UT stirring. CV and LSV for the ORR measurements were acquired for each sample.

Figure 7 shows the CVs of the three samples at the scan rate of 20 mV/s, with current density values related to the geometrical area of the support (5 mm). Overall, the main characteristics of platinoid metals are clearly observed in all cases, i.e., hydrogen, double layer and oxides regions. The electrochemically active surface area (EASA) of the catalysts can be calculated from such CV plots by obtaining the electric charge under the hydrogen desorption peaks (after correction of the double layer charging) region and considering 210 $\mu C/cm^2$ as the charge required to adsorb a monolayer of hydrogen.

With this approach, the EASA of the Pd(UT)-Pt nanostructure is calculated to be 1.98 cm^2, while the EASA values for Fe_3O_4(USS)-Pt and Fe_3O_4(UT)-Pt are 0.15 and 0.21 cm^2, respectively. This means that the EASA for Pd(UT)-Pt is about 13 and 9 times larger than the values obtained for Fe_3O_4(USS)-Pt and Fe_3O_4(UT)-Pt. This difference may suggest a more optimal physicochemical interaction between Pd and Pt to promote the formation of bimetallic nanostructures.

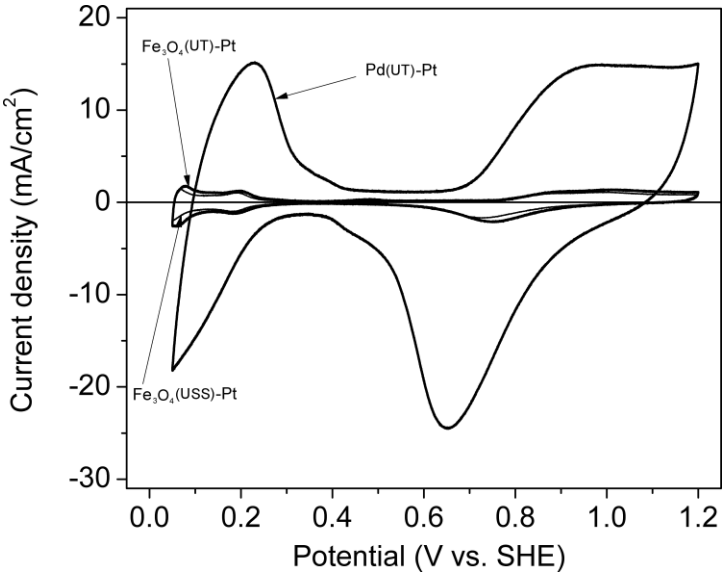

Figure 7. CVs of the Fe_3O_4(UT)-Pt, Fe_3O_4(USS)-Pt and Pd(UT)-Pt systems. Scan rate: 20 mV/s.

Figure 8 shows the LSVs of the ORR at the Pd(UT)-Pt nanostructure at the slow scan rate of 2 mV/s, also considering the geometrical area of the support. The different rotating rates (in rpm) are indicated. The increase in current density as the diffusion of species is higher can be clearly seen, indicating the selectivity of this material for the ORR. The high onset potential for the ORR at the Pd(UT)-Pt catalyst is of nearly 1.1 V vs SHE.

It can be observed that no ORR current density plateau is reached at this cathode material. Important cathodic peaks emerge in the 0.7-0.3 V range, somehow emulating the shape of the

curve in Figure 7 under N_2 atmosphere. This behavior is clearly unexpected because Pt is present in the catalyst. Such performance may be related to a low surface coverage of O_{ads} due to the morphological or structural characteristics of the cathode. Further studies are under active investigation to elucidate the shape of the ORR curve at this Pt-based material, including HRTEM analysis of Pd-Pt. This should give detailed information of the morphological configuration of the bimetallic cathode.

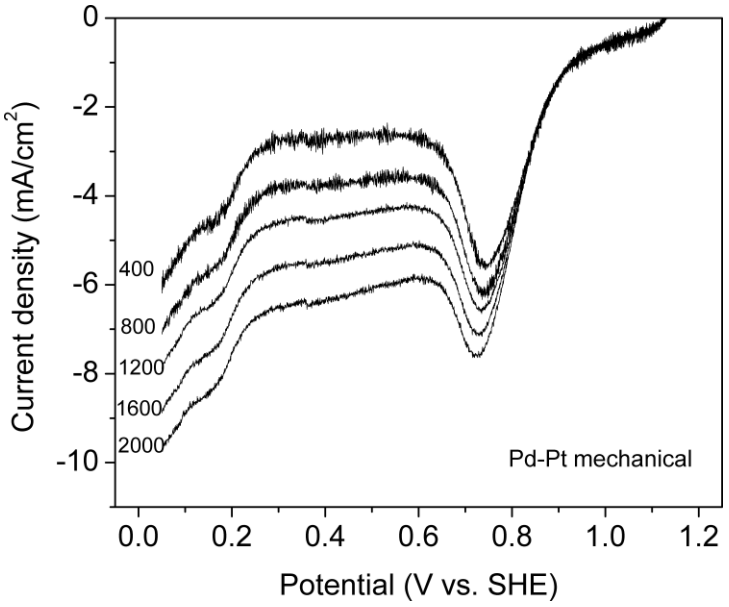

Figure 8. LSVs of the ORR at Pd(UT)-Pt. Sweep rate: 2 mV/s.

Figures 9 and 10 show the LSVs of the ORR at the Fe_3O_4(UT)-Pt and Fe_3O_4(USS)-Pt systems, respectively. The scan rate in both cases is also 2 mV/s. Both bimetallic nanostructures show good catalytic activity for the ORR under hydrodynamic control. Overall, the voltamperograms in Figures 9 and 10 show similar current-potential characteristics, although the current densities of the ORR acquired from the magnetite-containing cathodes are lower than that obtained from the Pd(UT)-Pt nanostructure in Figure 8.

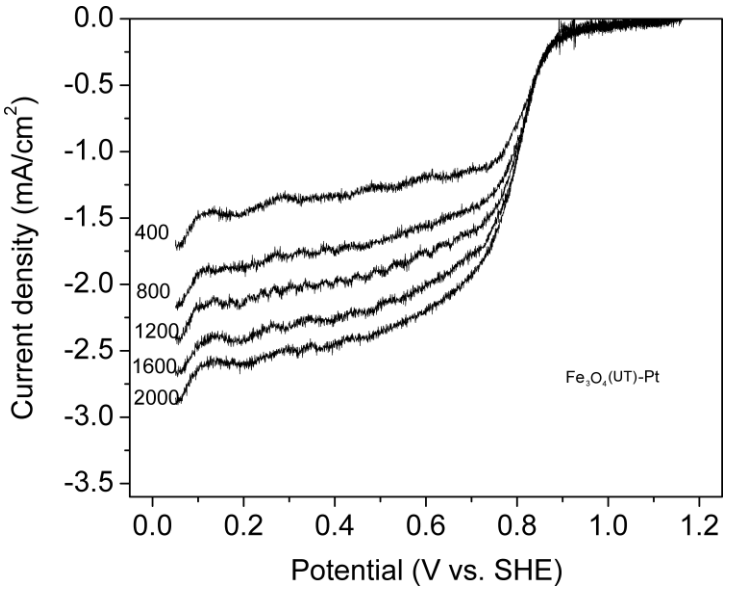

Figure 9. LSVs of the ORR at Fe_3O_4(UT)-Pt. Scan rate: 2 mV/s.

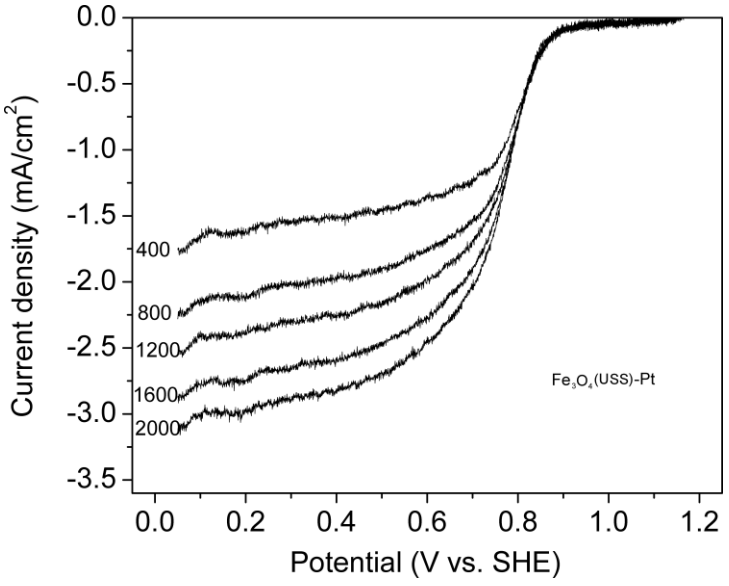

Figure 10. LSVs of the ORR at Fe_3O_4(USS)-Pt. Scan rate: 2 mV/s.

4. CONCLUSIONS

In this work we show that a good control on the reaction temperature in the simple methods (MS, UT, USS) used leads to a control of the structural parameters of the nanoparticles, which in turn affect the properties of the studied materials. The three methods are efficient to produce metallic and bimetallic materials with well defined XRD patterns and nanometric crystallite size.

The electrochemical characterization indicates that the EASA of the Pd-Pt nanostructure is about 13 and 9 times larger than those of the Fe_3O_4-Pt materials prepared by the different methods. The three nanostructures tested show a good catalytic activity for the ORR, although the cathodic current density is higher for the Pd-Pt system.

Further characterizations of the nanostructures currently being developed include HRTEM, EDAX and XPS analyses. The results will help us determine, among other properties, if we have core@shell systems.

5. ACKNOWLEDGMENTS

The authors thank the Mexican National Council for Science and Technology (CONACYT) for financial support through grant 79870 and the Redes Temáticas Program.

6. REFERENCES

[1] S. Alayoglu, A. U. Nilekar, M. Mavrikakis, B. Eichhorn, *Nature Materials*, **7**, 333-338 (2008).

[2] H. Wang, C. Xu, F. Cheng, M. Zhang, S. Wang, S. P. Jiang, *Electrochemistry Communications*, **10**, 1575–1578 (2008).

[3] N. V. Long, T. Asaka, T. Matsubara, M. Nogami, *Acta Materialia*, **59**, 2901-2907, (2011).

[4] K. Sasaki, J.X. Wang, H. Naohara, N. Marinkovic, K. More, H. Inada, R.R. Adzic, *Electrochimica Acta*, **55**, 2645–2652 (2010) .

[5] G. Wang, H. Wu, D. Wexler, H. Liu, O. Savadogo, *Journal of Alloys and Compounds*, **503**, L1–L4 (2010).

[6] D. Morales-Acosta, L.G. Arriaga, L. Alvarez-Contreras, S. Fraire Luna and F.J. Rodríguez Varela, *Electrochemistry Communications*, **11**, 1414-1417 (2009).

[7] Hui Wang, Rongfang Wang, Hao Li, Qunfang Wang, Jian Kang, Ziqiang Lei, *International Journal of Hydrogen Energy*, **36**, 839-848 (2011).